Electronic Supplementary Information:

Preparing $Bi_{12}SiO_{20}$ crystals at low temperature through nontopotactic solid-state transformation and improving its photocatalytic activity by etching

Qiaofeng Han,[a,*] Juan Zhang,[a] Xin Wang, Junwu Zhu[*]

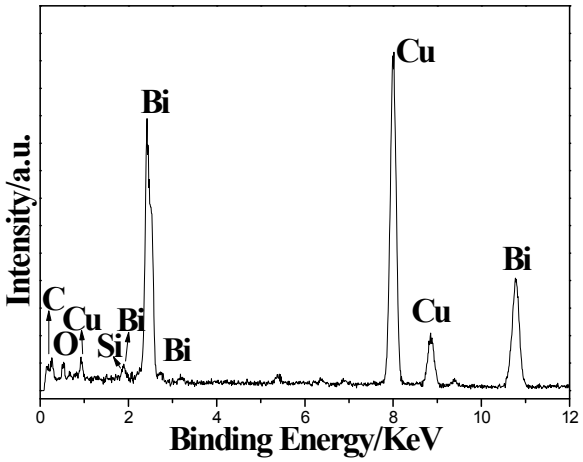

Figure S1 EDS spectrum of the as-prepared BSO microcrystallites.

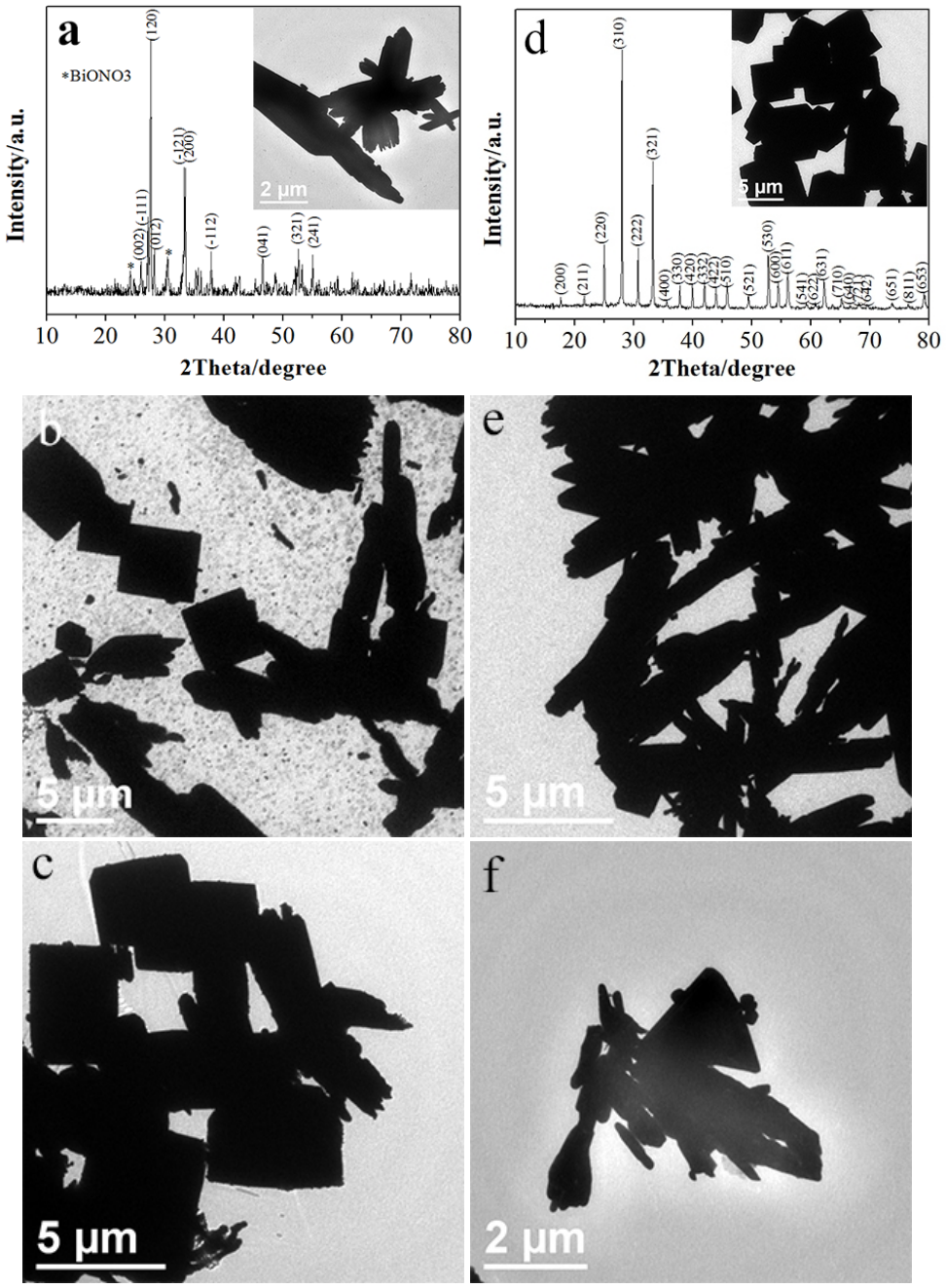

Figure S2 (a)-(d) XRD patterns and TEM images of the samples obtained at 70 °C in NaOH (3 M) solution with different reaction times: (a) 1 h, (b) 80 min, (c) 90 min and (d) 2 h; (e) and (f) TEM images of the products prepared at 50 °C for 3 h with 3 M and 5 M of NaOH, respectively.

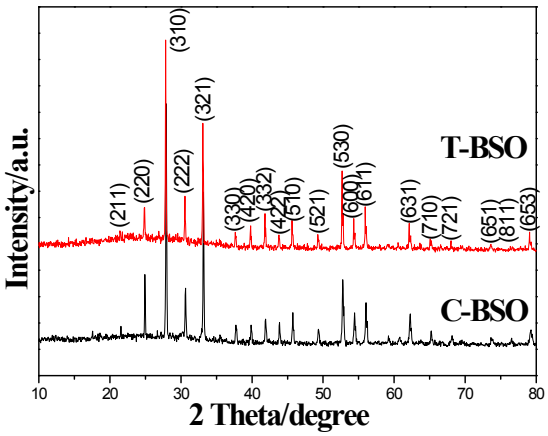

Figure S3 XRD patterns of cubic BSO (C-BSO) and trianglar pyramidal BSO (T-BSO) prepared at 3 M and 5 M of NaOH solution, respectively.

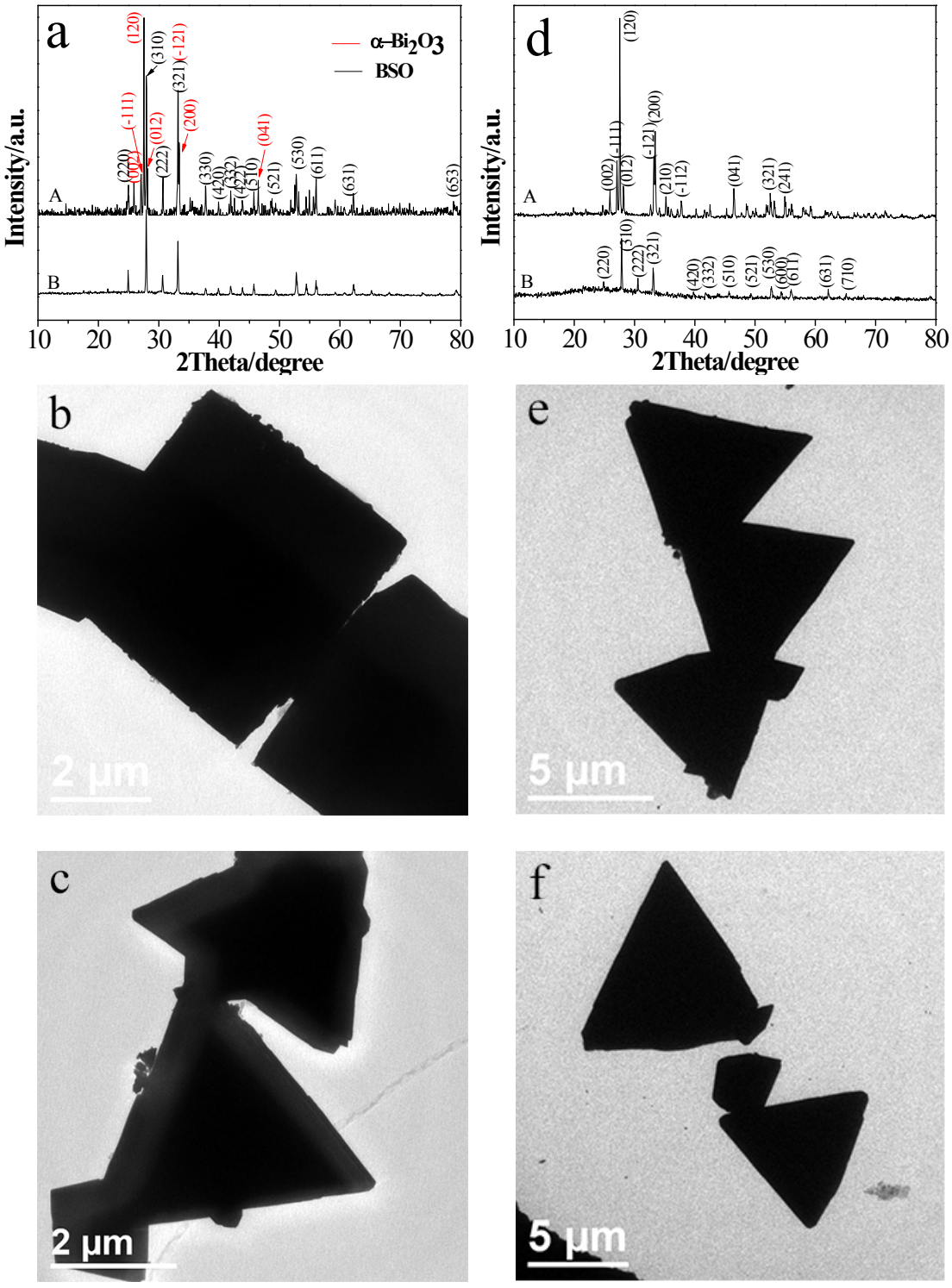

Figure S4 (a) XRD patterns of the products obtained from $(BiO)_2CO_3$ at 70 °C with 1 h (A) and 3 h (B) of reaction in 1.5 M of NaOH solution; (b) and (c) TEM images of BSO obtained from $(BiO)_2CO_3$ at 2 M and 3 M of NaOH solution, respectively; (d) XRD patterns of the products obtained from BiOCl at 70 °C with 50 min (A) and 3 h (B) of reaction in 5 M of NaOH solution; (e) and (f) TEM images of BSO obtained from BiOBr and α-Bi_2O_3 in 3M of NaOH solution, respectively.

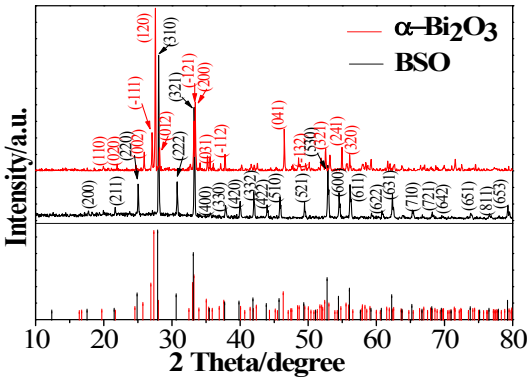

Figure S5 XRD patterns of α-Bi_2O_3 and BSO prepared after 1 and 3 h of reaction at 70 °C in NaOH (3 M) from $Bi(NO_3)_3$, respectively; the vertical stick below the patterns representing the standard diffraction data from JCPDS file for bulk BSO (No. 37-0485) and α-Bi_2O_3 (No. 65-2366).

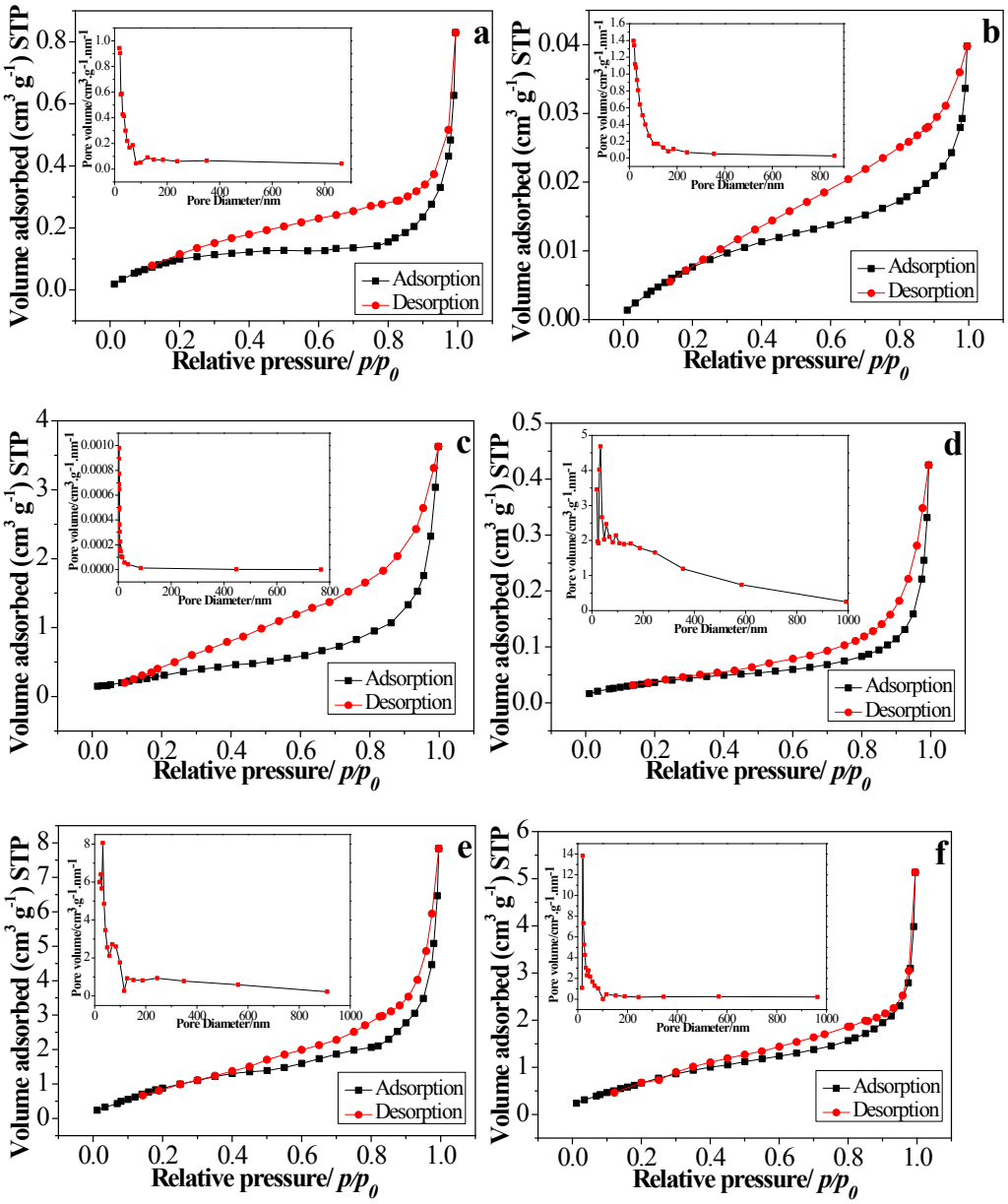

Figure S6 Typical nitrogen adsorption-desorption isotherms of the samples: (a) T-BSO, (b) C-BSO, (c) et-T-BSO, (d) et-C-BSO, (e) S-BOC, and (f) H-BOC; the insets are the corresponding pore-size distribution.

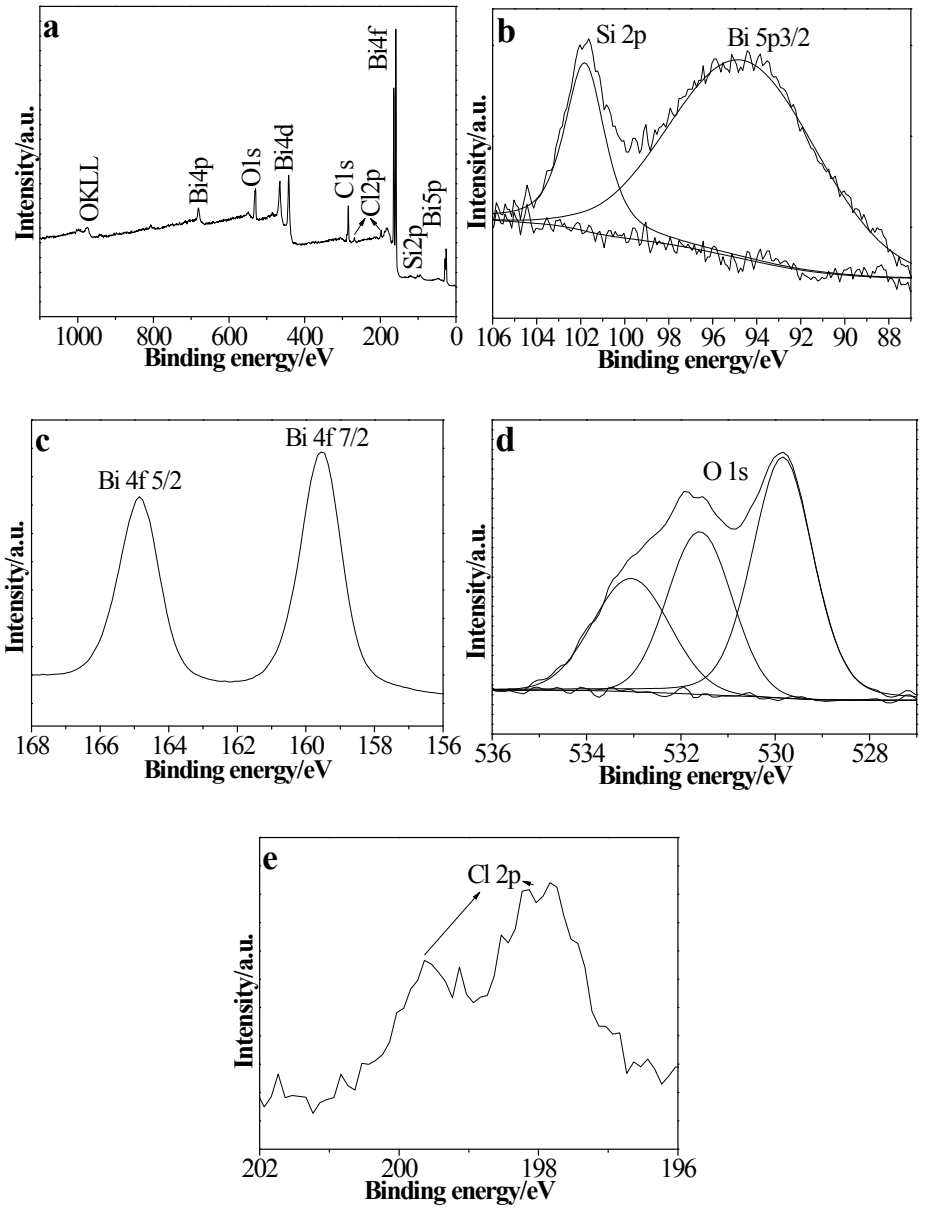

Figure S7 XPS spectra of et-C-BSO after etching in 0.1 M of HCl/HAc solution for 1 min: (a) survey, (b) Si 2p, (c) Bi 4f, (d) O 1s and (e) Cl 2p core level.

The survey spectra of et-C-BSO show the presence of Bi, O, C and Si elements as well as a trace amount of Cl (Fig. S7a). XPS spectra of Si 2p overlap with Bi 5p3/2 at high binding energy side (Fig. S7b) . The peak area of Si 2p significantly increases as compared to that before etching, indicating that bismuth removal through etching. The two characteristic bands of binding energies located in 158.9 and 164.2 eV can be

assigned to the spin orbital splitting of Bi (4f 7/2) and Bi (4f 5/2) in the BSO (Fig. S7c). The O 1s core level spectra of BSO can be fitted into three peaks (Fig. S7d). The band located at binding energies of 529.7 eV is attributed to oxygen atoms of Si-O. The higher peak at 531.5 eV is originated from Bi-O. The binding energy at 533.2 eV should be due to the presence of hydroxyl group (or adsorbed H_2O) on the surface of the BSO. The XPS spectra of Cl 2p show two weak peaks centered at about 197.8 and 199.6 eV, which can be assigned to the spin orbital splitting of Cl 2p 3/2 and Cl 2p 1/2, implying the presence of the impurity BiOCl (Fig. S7e).

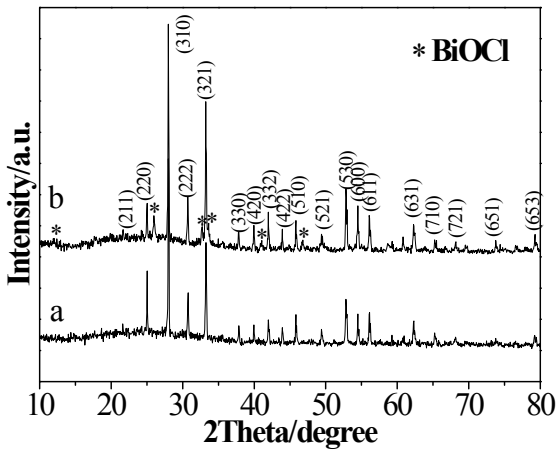

Figure S8 XRD patterns of the etched C-BSO obtained after 1 min of etching reaction in 0.1 M of (a) HCl/HAc and (b) HCl/H_2O solution.

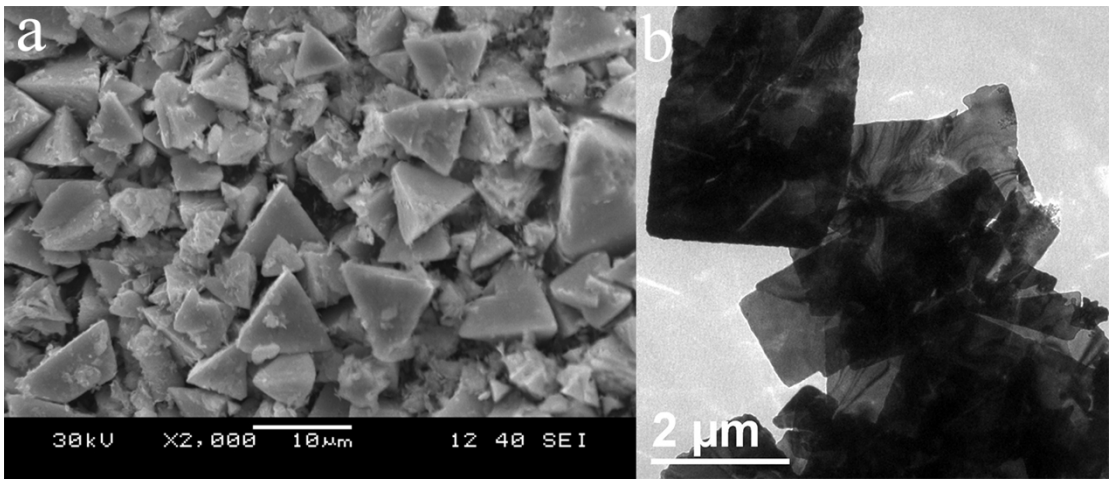

Figure S9 (a) SEM image of et-T-BSO etched in 0.1 M of HCl/HAc solution for 1 min; (b) TEM image of BiOCl nanosheets (S-BOC) obtained through etching reaction in 6 M of HCl/HAc solution (v/v = 1:1).

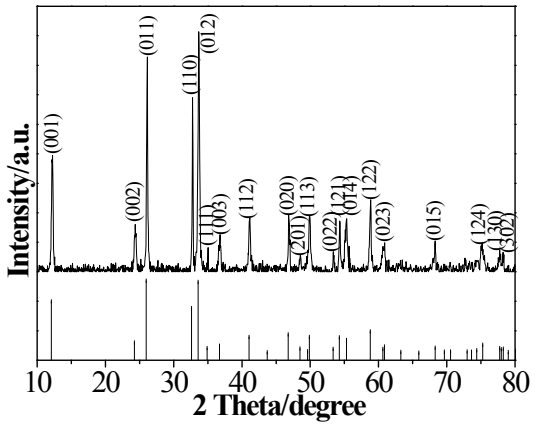

Figure S10 XRD pattern of BOCl hierarchitectures (H-BOC) prepared after 3 min of etching reaction in 1.2 M HCl/HAc solution, and vertical sticks below the pattern representing the standard diffraction data from JCPDS file for bulk BOCl (No. 73-2060).

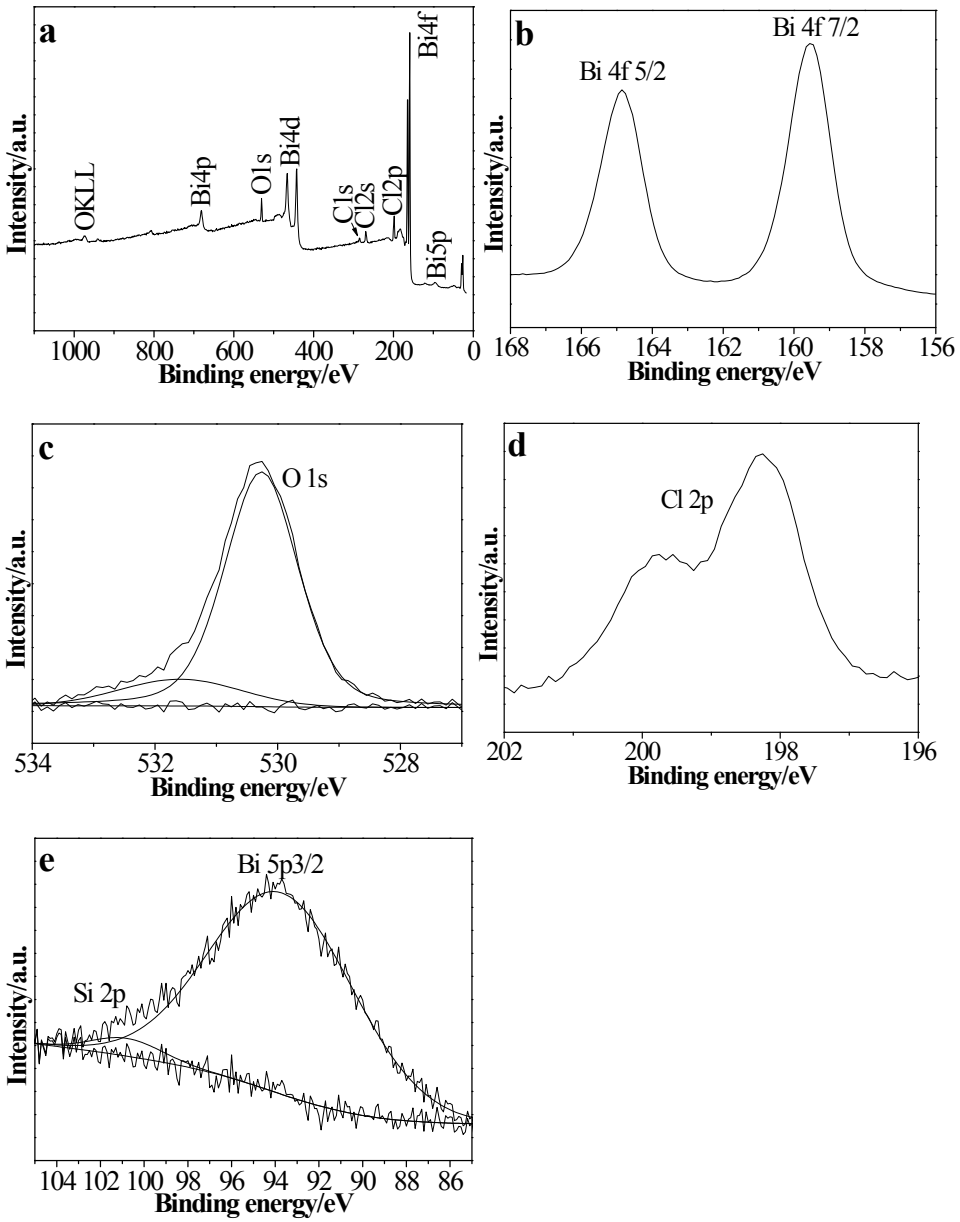

Figure S11 XPS spectra of H-BOC: (a) survey, (b) Bi 4f, (c) O 1s, (d) Cl 2p and (e) Bi 5p core level.

The XPS spectra of Bi 4f show two characteristic bands of energies located at 158.9 and 164.2 eV, corresponding to the spin orbital splitting of Bi (4f 7/2) and Bi (4f 5/2) in the H-BOC (Fig. S11b). The O 1s core level spectra of H-BOC can be fitted into two peaks (Fig. S11c). The band located at binding energies of 529.8 eV is attributed to oxygen in the BiOCl crystal lattice. The higher peak at 531.6 eV is originated from

hydroxyl group on the surface of the BiOCl. The Cl 2p core level spectra show two characteristic bands located at 198.2 and 199.8 eV, which can be assigned to the spin orbital splitting of Cl 2p 3/2 and Cl 2p 1/2 in the BiOCl (Fig. S11d). A very small peak centered at 101.0 eV overlapping with Bi 5p 3/2 spectrum at high binding energy side can be attributed to Si 2p core level, indicating element Si was almost completely removed as compared to Si 2p XPS spectra of BSO.

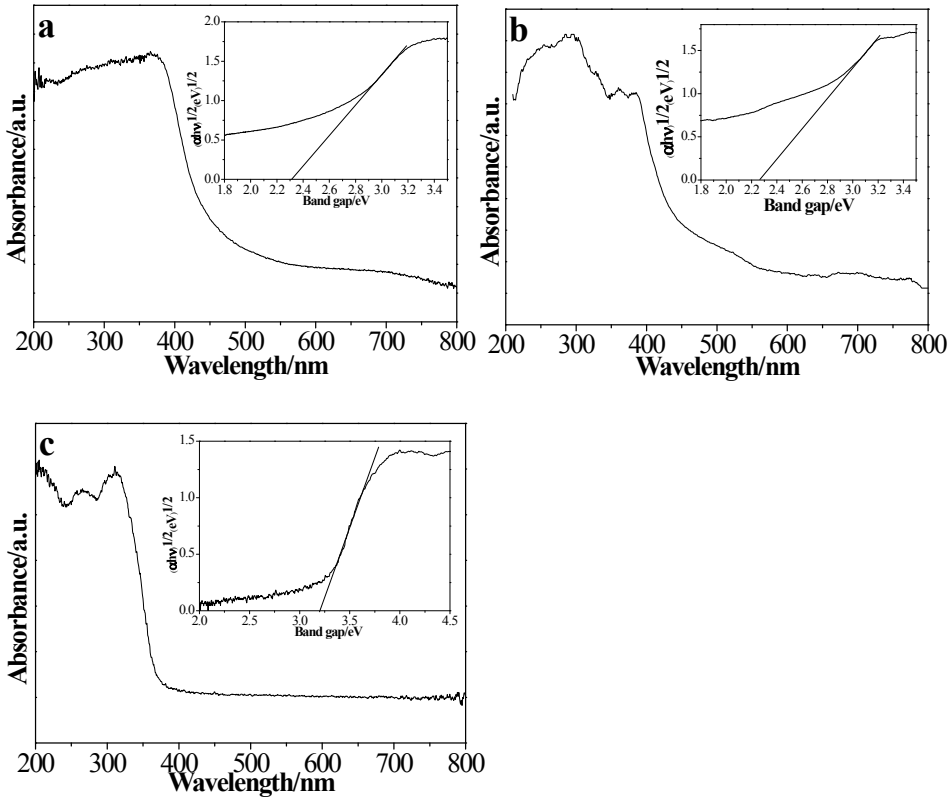

Figure S12 DRS spectra of the samples: (a) T-BSO, (b) et-T-BSO and (c) S-BOC; the insets showing their plots of $(\alpha hv)^{1/2}$ versus photon energy (hv).

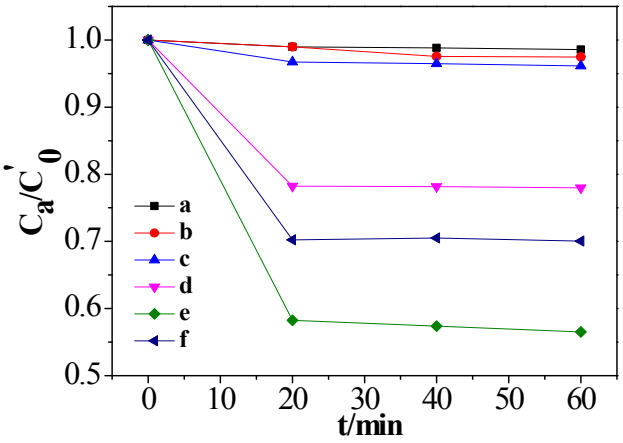

Figure S13 Time profiles of adsorption of RhB over the samples: (a) T-BSO, (b) C-BSO, (c) et-T-BSO, (d) et-C-BSO, (e) S-BOC, and (f) H-BOC, where C'_0 and C_a respectively represent initial concentration of RhB and concentration after adsorption for a certain time.

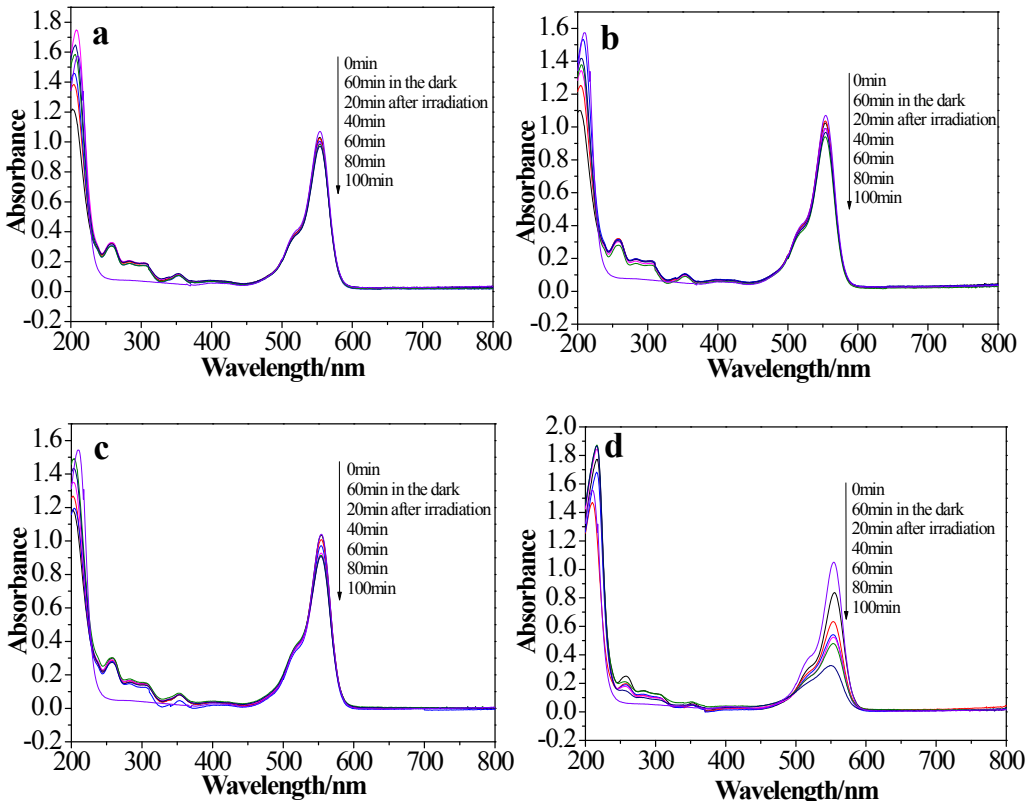

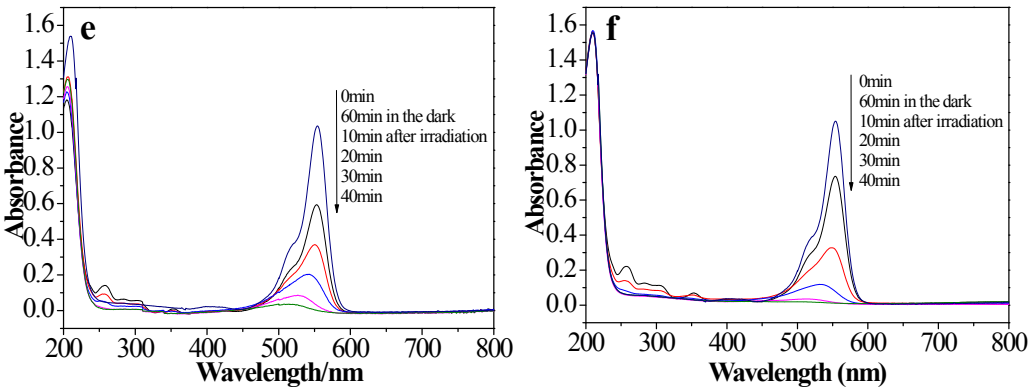

Figure S14 The temporal evolution of the absorption spectra of RhB under visible light over various catalysts: (a) T-BSO, (b) C-BSO, (c) et-T-BSO, (d) et-C-BSO, (e) S-BOC and (f) H-BOC.

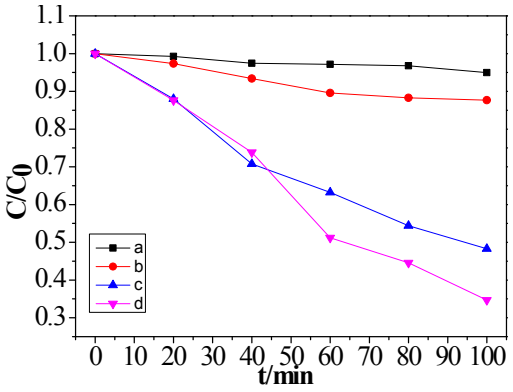

Figure S15 Influence of etchant concentration and etching time on photocatalytic activity of T-BSO under visible light: (a) 0.05 M, (b) 0.1 M, and (c) 0.2 M HCl for 1 min; (d) 0.1 M HCl for 2 min.

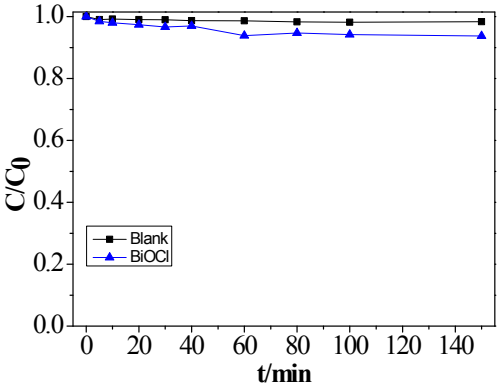

Figure S16 Photocatalytic efficiency of SA over H-BOC with visible light irradiation time.

Table S1 Degradation rate (DR) and degradation time (t) of RhB over the BiOCl catalysts with various morphology and dosages under UV and visible light

Morphology	Dyes (mg)	DR (%)	Dosage (g)	t (min)
flower-like [b]	1	100 [1]	0.05	50
desertrose-like [b]	0.479	100 [2]	0.01	20
micro-flowers [b]	2	100 [3]	0.02	20
Nanosheets [a]	1	81 [4]	0.02	32
hierarchitectures [a]	2	100 [5]	0.02	70
hollow spheres [a]	2	100 [6]	0.1	75
Nanodisks [b]	0.6	100 [7]	0.02	120
Microsphere [a]	1.2	100 [8]	0.06	70
Black BOC [b]	1	98 [9]	0.02	60
flower-like [b, c]	0.289	100	0.02	40

([a] UV light, [b] Visible light, [c] This study)

1 L. Chen, S. F. Yin, R. Huang, Y. Zhou, S. L. Luo and C. T. Au, *Catal. Commun*., 2012, **23**, 54.

2 G. Cheng, J. Xiong and F. J. Stadler, *New J. Chem*., 2013, **37**, 3207.

3 D. H. Wang, G. Q. Gao, Y. W. Zhang, L. S. Zhou, A. W. Xu and W. Chen, *Nanoscale*, 2012, **4**, 7780.

4 L. Ye, L. Zan, L. Tian, T. Peng and J. Zhang, *Chem. Commun.,* 2011*,* **47**, 6951.

5 L. P. Zhu, G. H. Liao, N. C. Bing, L. L. Wang, Y. Yang and H. Y. Xie, *CrystEngComm*, 2010, **12**, 3791.

6 K. Zhang, J. Liang, S. Wang, J. Liu, K. Ren, X. Zheng, H. Luo, Y. Peng, X. Zou, X. Bo, J. Li and X. Yu, *Cryst. Growth Des*., 2012, **12**, 793.

7 X. Zhang, X. W. Wang, L. W. Wang, W. K. Wang, L. L. Long and H. Q. Yu, *ACS Appl.*

Mater. Interfaces, 2014, **6**, 7766.

8 F. Chen, H. Liu, S. Bagwasi, X. Shen and J. Zhang, *J. Photochem. Photobiol A*, 2012, **215**, 76.

9 L. Ye, K. Deng, F. Xu, L. Tian, T. Peng and L. Zan, *Phys. Chem. Chem. Phys.*, 2012, **14**, 82.

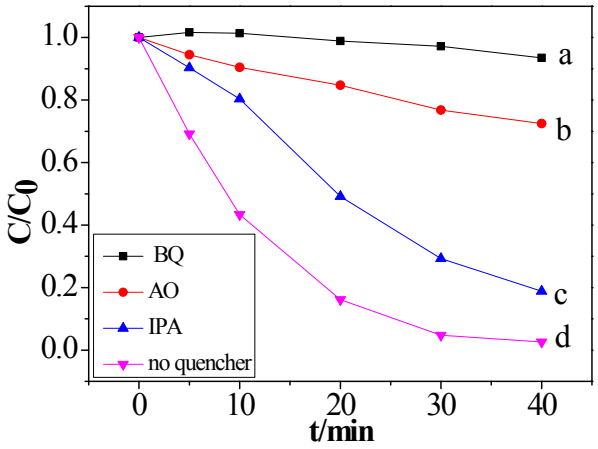

Figure S17 Photodegradation efficiency of RhB over H-BOC in the presence of 1 mM of: (a) BQ, (b) AO, (c) IPA and (d) no quencher.

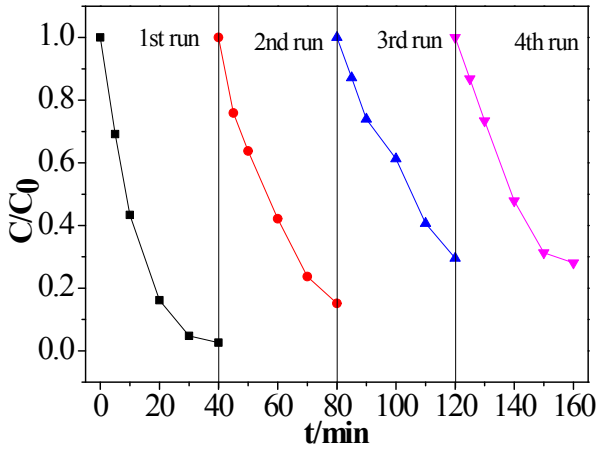

Figure S18 Cycling tests of the H-BOC catalyst under visible light.

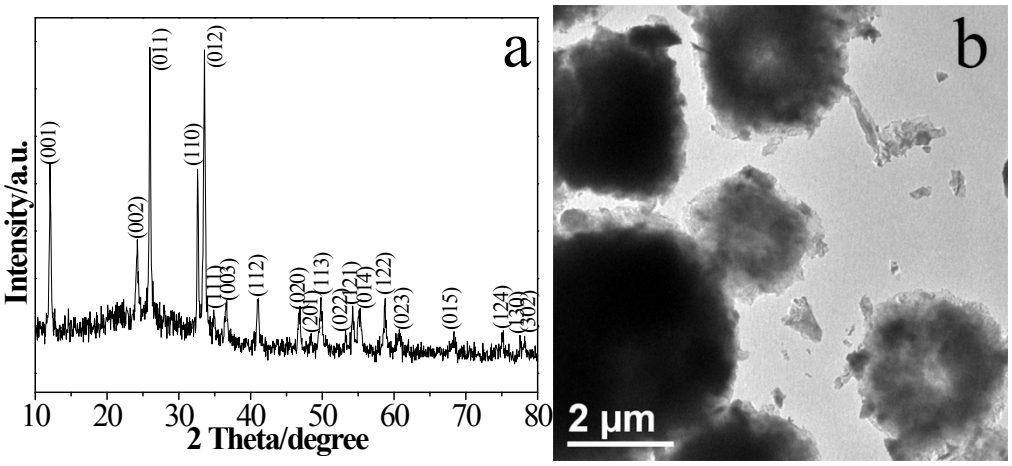

Figure S19 (a) XRD pattern and (b) TEM image of H-BOC catalyst after four photocatalytic cycles.